Supporting Information

Metastable Cubic Cu_3SbS_3: A Facile Solution-Phase Access to a Kinetic Polymorph

Rittika Dhar[1], Anil Kumar B. M.[1], Pranav Negi[2], Shuva Biswas,[3]
Dirtha Sanyal[4,5] and Satya N. Guin[1,*]

[1]*Department of Chemistry, Birla Institute of Technology and Science Pilani, Hyderabad Campus, Jawahar Nagar, Hyderabad 500078, India*

[2]*Department of Chemistry, Indian Institute of Science Education and Research Bhopal, Bhopal 462066, India*

[3]*New Chemistry Unit, Jawaharlal Nehru Centre for Advanced Scientific Research (JNCASR), Jakkur P.O., Bengaluru 560064, India*

[4]*Variable Energy Cyclotron Centre, 1/AF Bidhannagar, Kolkata 700064, India*

[5]*Homi Bhabha National Institute, Training School Complex, Anushakti Nagar, Mumbai 400094, India*

[*]Email: *satyanarayan.g@hyderabad.bits-pilani.ac.in*

Experimental section

Materials. Nanocrystalline Cu_3SbS_3 was synthesised using copper (II) nitrate trihydrate (99.5%, AR, SRL), antimony acetate (99.99%, Sigma-Aldrich), sulfur powder (reagent grade, Sigma-Aldrich), and 2-amino-ethan-1-ol (99+%, TCI). For the bulk Cu_3SbS_3 synthesis, elemental precursors were used: copper shot (99.9999%, Alfa Aesar), antimony shot (99.999%, Sigma-Aldrich), and sulfur powder (reagent grade, Sigma-Aldrich). All the chemicals were used as received without any further purification.

Synthesis of nanocrystalline Cu_3SbS_3. In a typical one-pot synthesis, $Cu(NO_3)_2 \cdot 3H_2O$ (146.3 mg, 0.605 mmol), $Sb(CH_3COO)_3$ (60 mg, 0.200 mmol), and sulphur powder (19.4 mg, 0.604 mmol) were accurately weighed and transferred into a 25 mL three-neck round-bottom flask alongside 10 mL 2-Amino-1-ethanol. The reaction mixture was heated to 150 °C under normal atmospheric conditions with constant stirring and continued for 30 min. After cooling naturally to room temperature, the resulting dark brown precipitate was collected, washed several times with ethanol, and dried in a fume hood. To prepare the nanocrystalline Cu_3SbS_3 for thermoelectric measurements, the powder was subjected to a hydrazine treatment. This involved vigorous stirring in a 3:1:4 volumetric mixture of chloroform, methanol, and hydrazine hydrate until precipitation occurred. The resulting product was then washed with ethanol and dried.

Synthesis of bulk Cu_3SbS_3. Stoichiometric amounts of high-purity elements Cu, Sb and sulfur were weighed and transferred to a quartz tube. The tube was flame sealed under high vacuum (10^{-5} Torr) and slowly heated to 900 °C over a period of 12 hours, soaked at this temperature for 48 hours, and finally quenched in ice-cold water.

Powder X-ray Diffraction (PXRD). A Rigaku Ultima IV diffractometer with Cu $K\alpha_1$ radiation (λ = 1.5418 Å) was used for the room temperature powder X-ray diffraction (PXRD) data collection of all the samples. Temperature-dependent PXRD was performed using a PANalytical Empyrean diffractometer with CuKα radiation (λ = 1.5406 Å). Rietveld refinement was performed using the FullProf package.[1] The obtained R_p and R_{wp} were 10.1 and 12.9, respectively.

Field Emission Scanning Electron Microscopy (FESEM). FESEM imaging was performed using the FEI-Apreo LoVac. Energy dispersive spectroscopy (EDX) was performed with the coupled Oxford X-Max EDX. Backscattered FESEM images were taken using an Apreo 2S, SEM, Thermo Scientific microscope.

Transmission electron microscopy (TEM). TEM imaging was done using a Jeol JEM F200 Multipurpose electron microscope.

X-ray photoelectron spectroscopy (XPS). XPS measurements were done using a Thermo Scientific K-Alpha (Al-Kα monochromator, 1486.6 eV) XPS instrument.

Differential Scanning Calorimetry (DSC). DSC measurements were performed on a NETZSCH DSC 214 instrument from room temperature (RT) to 773 K at a heating rate of 5 K min^{-1} under a nitrogen flow of 250 mL min^{-1}.

Band Gap Measurement. The optical diffuse reflectance spectra of nanocrystalline and bulk Cu_3SbS_3 were recorded using a Jasco UV-670 UV-vis-NIR spectrophotometer in the wavelength range of 300-2200 nm. The Kubelka-Munk equation: $\alpha / S = (1 - R)^2 / 2R$, where R denotes reflectance, while α and S represent absorption and scattering coefficients, respectively, was used to calculate absorption (α/S) from the reflectance data. The optical band gap was measured from the plot of α/S (a. u.) vs E (eV).

Positron annihilation spectroscopy. The positron annihilation lifetime (PAL) has been done by standard γ-γ coincidence technique[2,3]. Two ultrafast BaF_2 scintillates (25 mm × 25 mm) coupled with two XP2020Q photomultiplier tubes have been used for the two g-ray detectors. The timing resolution of the positron lifetime spectrometer is about 220 ps, measured with a ^{60}Co gamma-emitting source (with the proper positron window settings). For the positron source a 8 micro-Curie $^{22}NaCl$ encapsulated in a 6-micron-thick mylar film has been used. The source component (self-annihilation of positrons inside the source) has been evaluated with a 99.9999 % pure Al single crystal. PATFITT computer programme has been used to deconvolute the positron lifetime spectrum. The positron lifetime components have been estimated with the proper source correction.

Coincidence Doppler broadening (CDB) studies have been carried out with two identical HPGe detectors (model number PGC 1216sp of DSG, Germany, of 12 % efficiency, having an energy resolution of 1.15 keV at 514 keV of ^{85}Sr). The high background suppressed (peak to background ratio ~ 10^5: 1) coincidence Doppler broadening spectra (using the ± ΔE

selection)[4]have been recorded in a dual ADC-based multiparameter data acquisition system (Model number MPA-3 of FAST ComTec, Germany). For each CDB spectrum, a total of 10^7 coincidence counts has been recorded.

Thermoelectric measurements. Nanocrystalline Cu_3SbS_3 was hot pressed into typical coins of 2mm thickness by employing graphite dies of 10 mm diameter under the axial pressure of 50 MPa for 30 minutes at 523 K. The Density of the hot-pressed sample was found to be ~ 90% of the theoretical density (4.967 g cm^{-3}). Thermal conductivity (κ) was calculated using the relation $\kappa = DC_p\rho$, where D is the thermal diffusivity, Cp is the specific heat capacity, and ρ is the density of the material. Thermal diffusivity was directly measured with NETZSCH LFA 457; Specific heat capacity was determined indirectly with the Pyroceram 9606 as a reference from NETZSCH LFA 457 in the temperature range of 303 to 723 K. Electrical resistivity and Seebeck coefficient were measured on Linseis LSR-3 under helium atmosphere in the temperature range of 336 to 725 K.

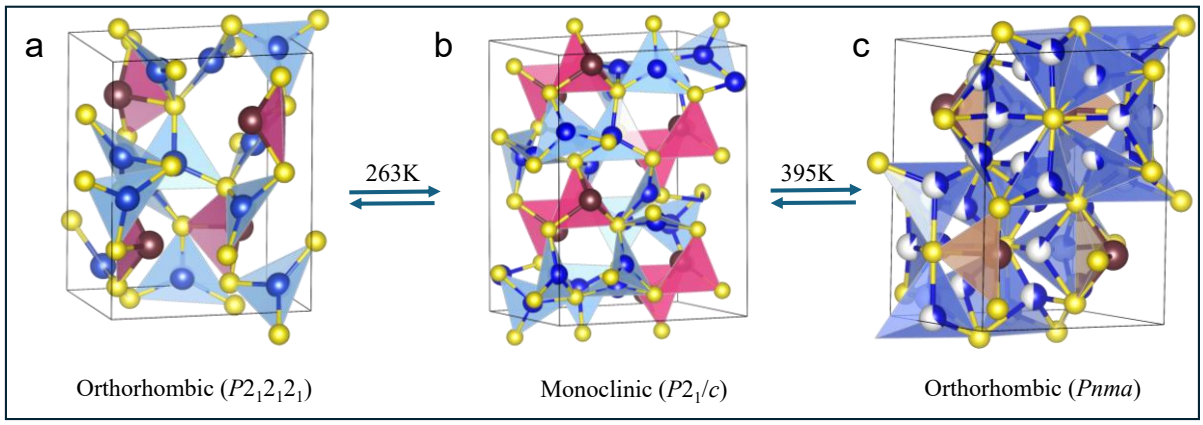

Fig. S1 Temperature-dependent crystal structural evaluation of Cu_3SbS_3: (a) Wittichenite (space group $P2_12_12_1$, <263 K), (b) Skinnerite ($P2_1/c$, 263–395 K), and (c) orthorhombic Cu_3SbS_3 (*Pnma*, >395 K).

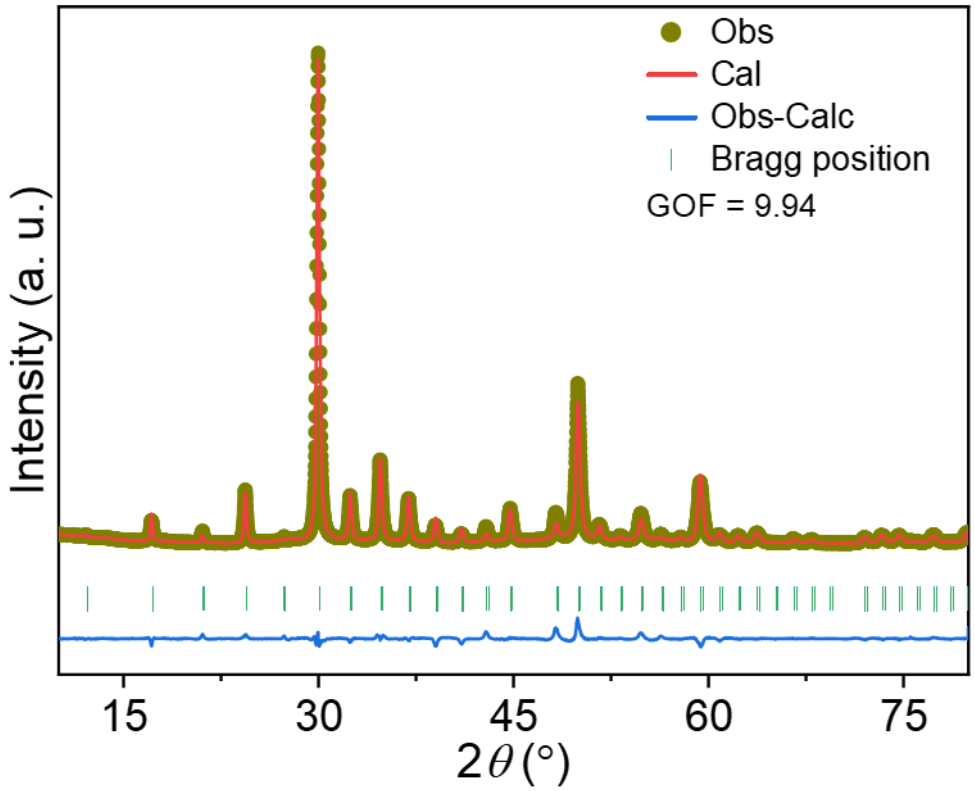

Fig. S2 Rietveld refinement of the room temperature powder XRD pattern of as-synthesised nanocrystalline cubic Cu_3SbS_3. The refined lattice parameter is $a = b = c = 10.320706$ Å.

Table S1 Structural parameters of the Rietveld refinement

Atom	X	Y	Z	U_{iso}
Cu1	0.25	0.5	0	0.00848
Cu2	0.21922	0.00	0.0	0.01050
Sb	0.26980	0.26980	0.26980	0.00751
S	0.10628	0.10628	0.37285	0.00744

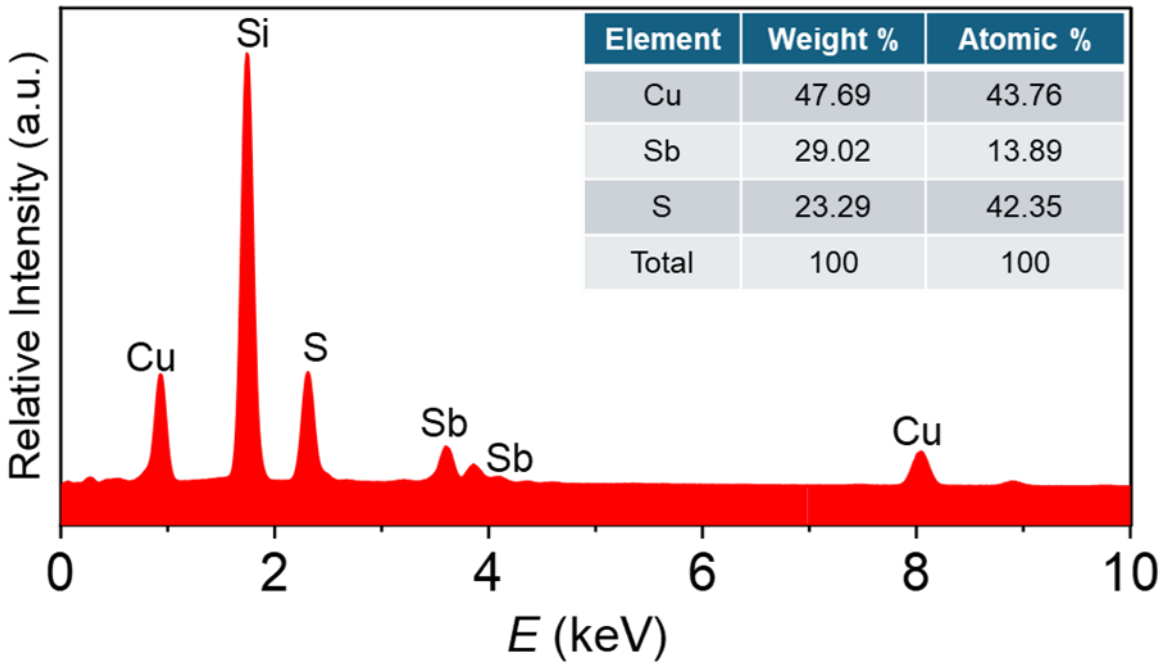

Element	Weight %	Atomic %
Cu	47.69	43.76
Sb	29.02	13.89
S	23.29	42.35
Total	100	100

Fig. S3 EDX spectrum of nanocrystalline Cu_3SbS_3, with the corresponding elemental composition shown in the inset.

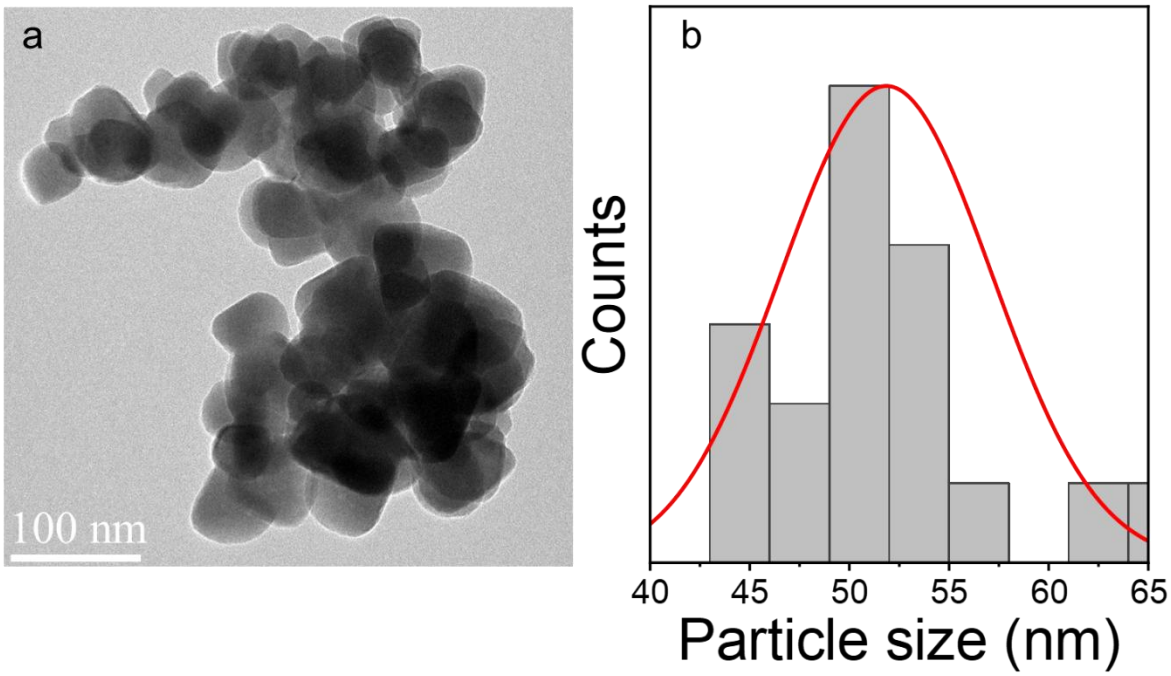

Fig. S4 (a) Additional TEM image of Cu_3SbS_3 nanocrystals and (b) the corresponding particle size distribution histogram.

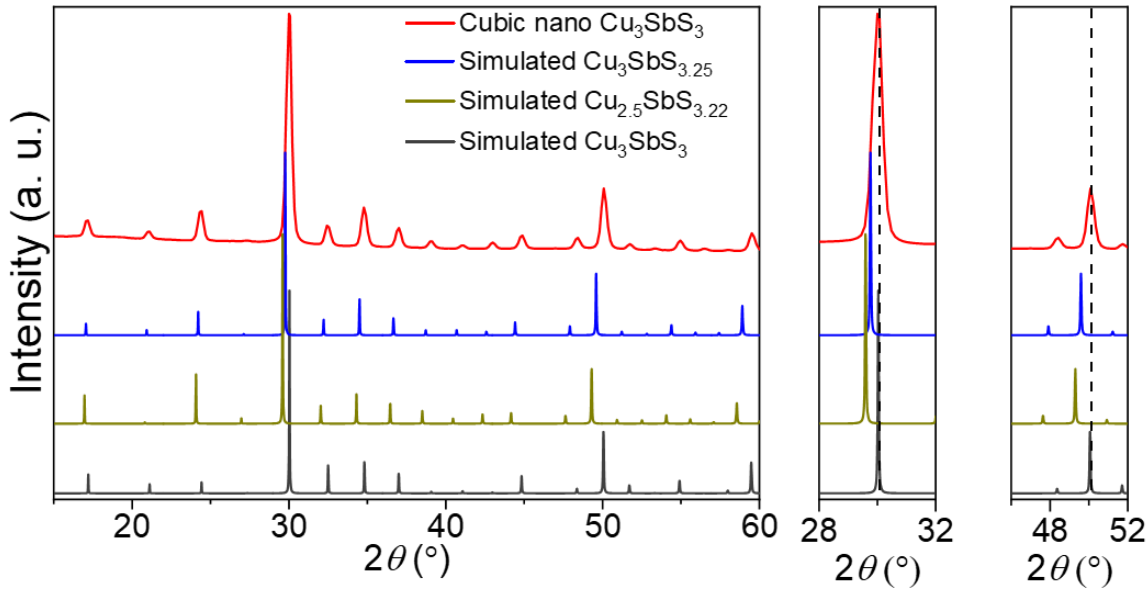

Fig. S5 Room-temperature PXRD pattern of as-synthesised cubic nanocrystalline Cu_3SbS_3 compared with its simulated pattern, pristine tetrahedrite ($Cu_3SbS_{3.25}$) and defect-stabilised tetrahedrite ($Cu_3SbS_{3.22}$) which indicates as-synthesised phase matches well with cubic Cu_3SbS_3.

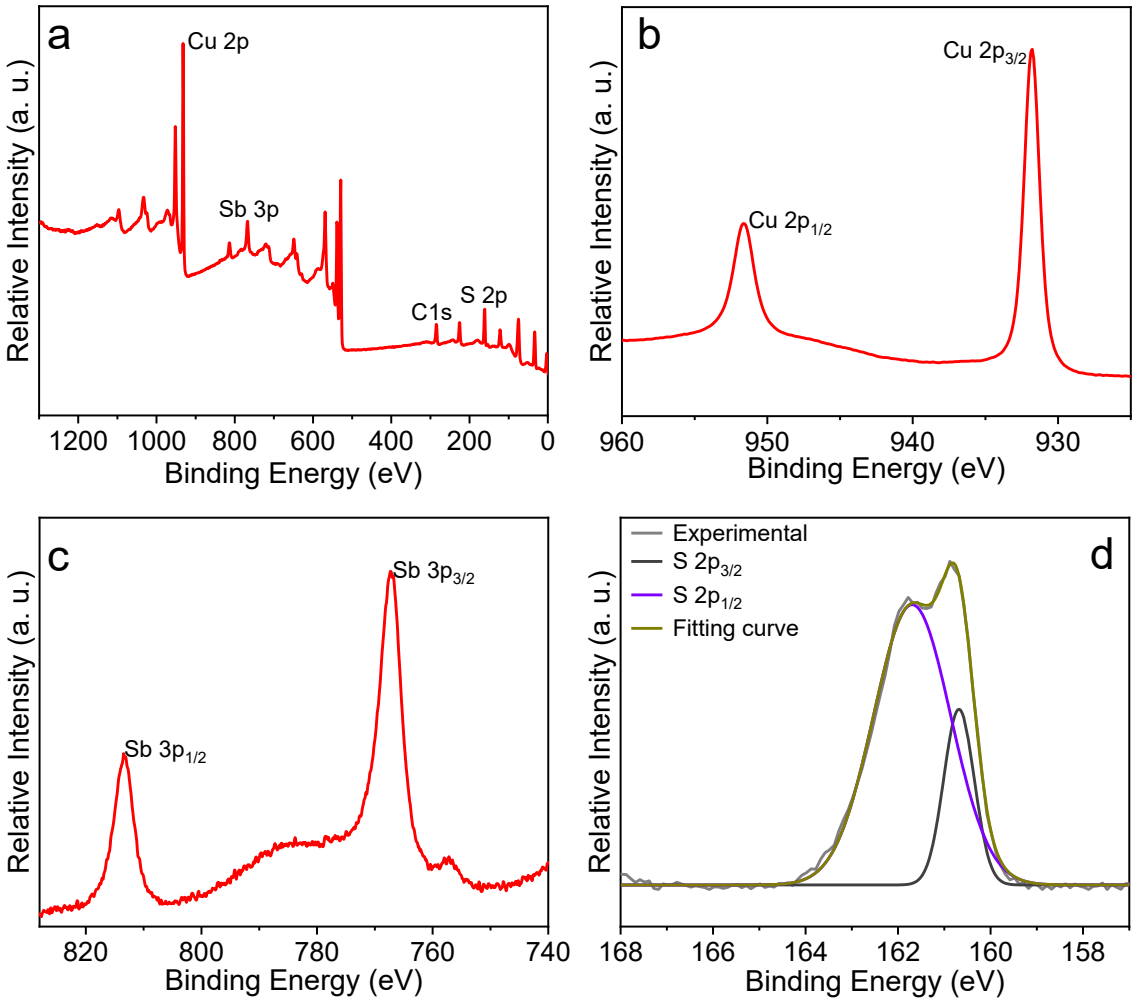

Fig. S6 XPS spectra of as-synthesised Cu_3SbS_3 nanocrystals: (a) survey scan, (b) Cu 2p, (c) Sb 3p, and (d) S 2p spectra. The doublet of S 2p has been fitted using a Gaussian model with an excellent goodness of fit (R^2) value of 0.998.

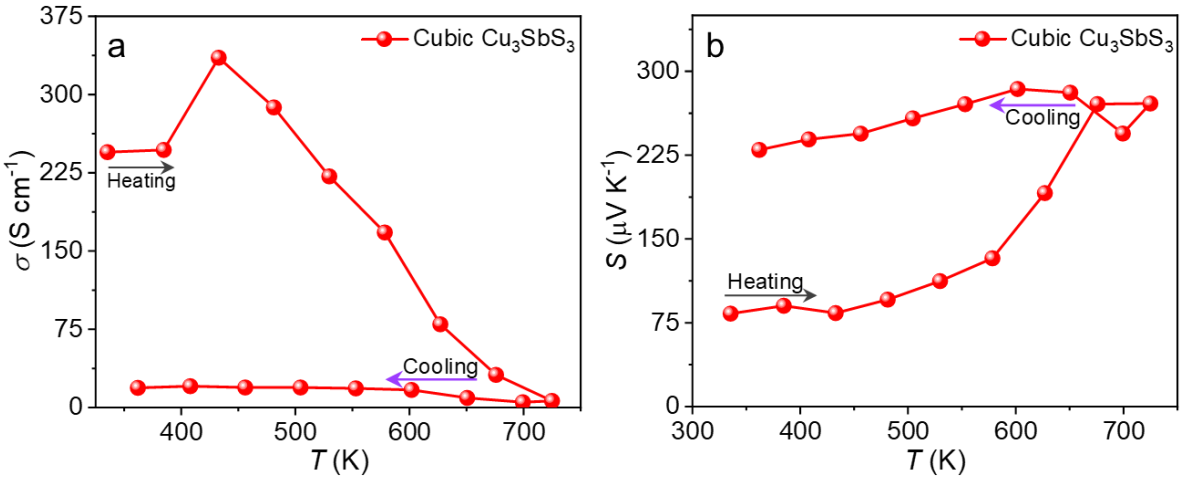

Fig. S7 Temperature-dependent (a) electrical conductivity, and (b) Seebeck coefficient of nanocrystalline Cu_3SbS_3 during a heating-cooling cycle, showing an irreversible nature.

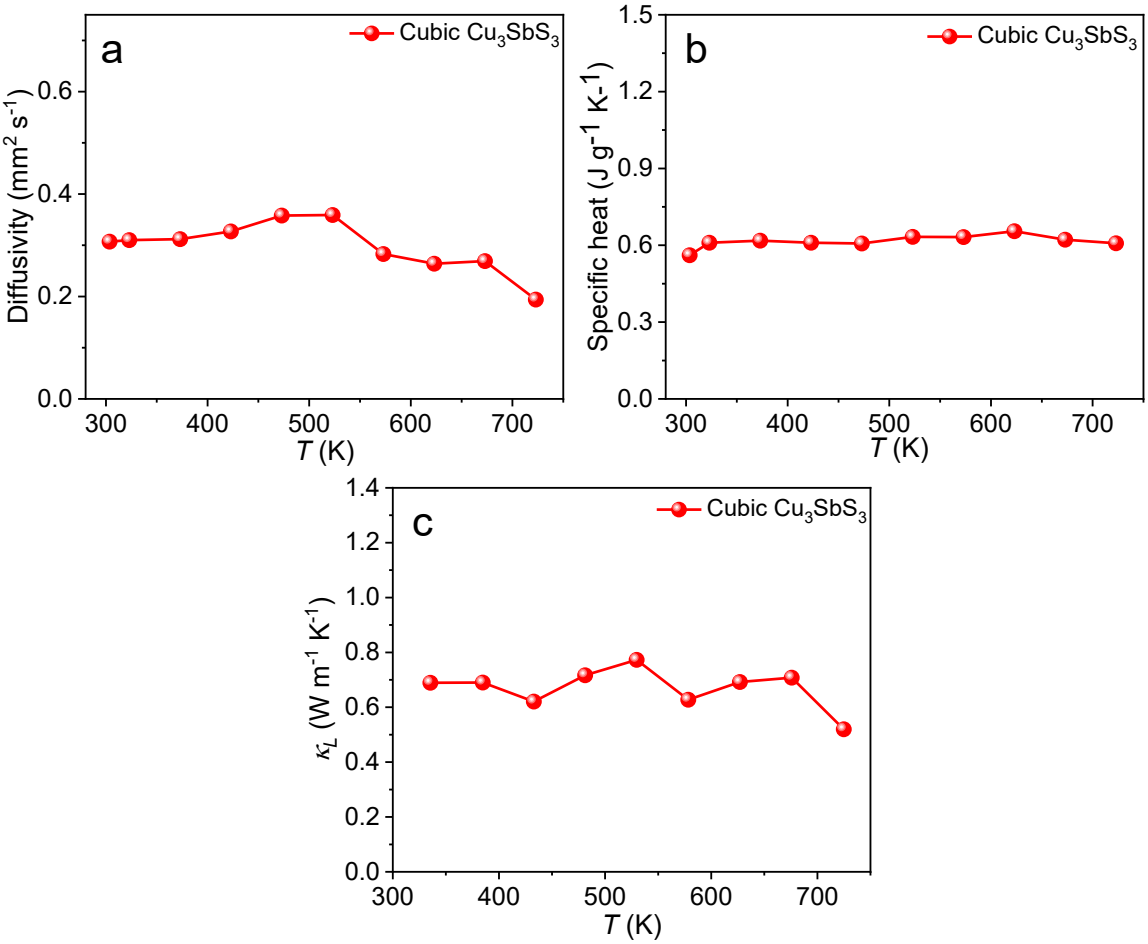

Fig. S8 Temperature-dependent (a) thermal diffusivity, (b) Specific heat capacity (*Cp*), (c) lattice thermal conductivity (κ_L), *Cp* estimated using Dulong-Petit limit is ~0.427 J g^{-1} K^{-1}.

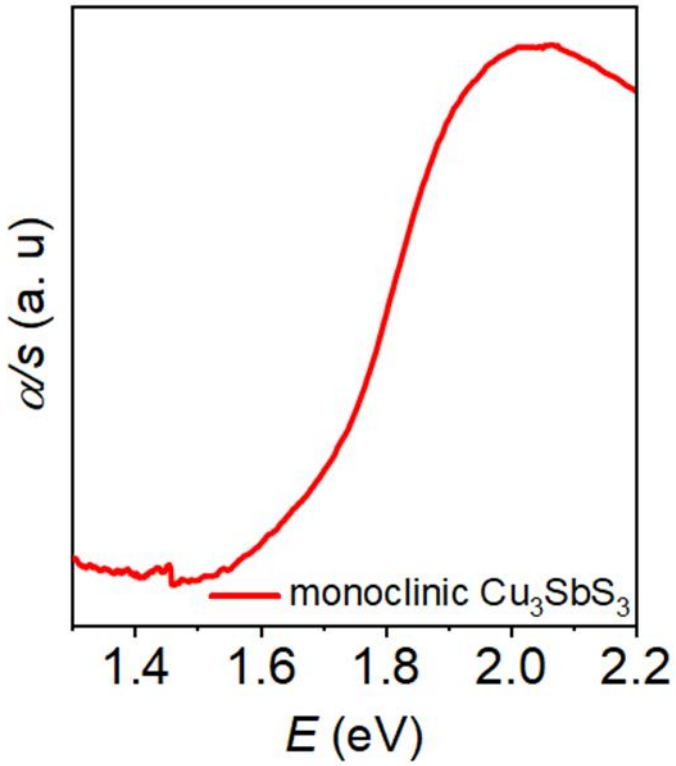

Fig. S9 Optical absorption spectra of monoclinic bulk Cu_3SbS_3 measured at room temperature.

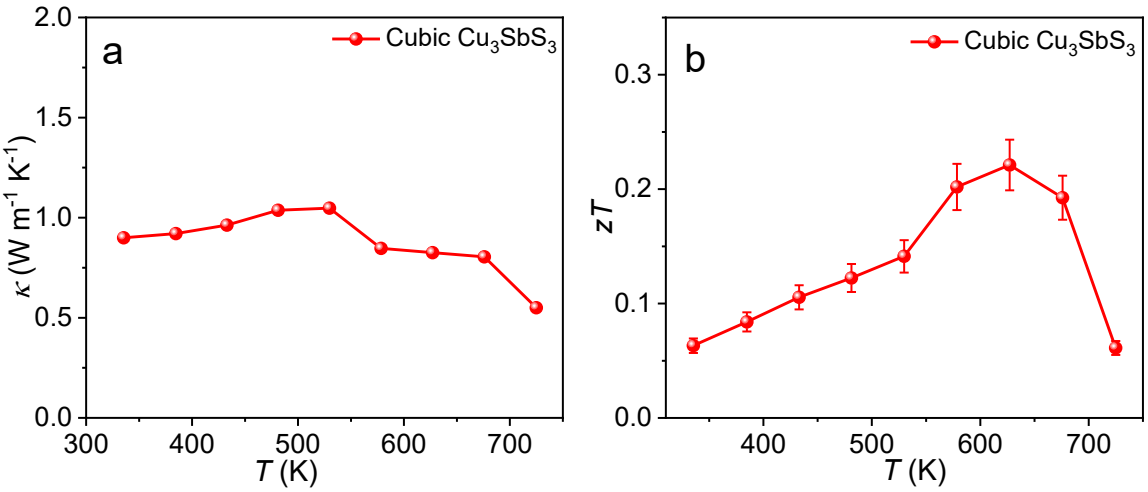

Fig. S10 Temperature-dependent (a) thermal conductivity (κ_L), (b) thermoelectric figure of merit (zT) of nanocrystalline Cu_3SbS_3 after porosity correction.

Since the sample have ~90 % of the theoretical density, we have also performed the porosity correction to correct the κ value using the formula given below:[5]

$$\kappa_m/\kappa = (1- \varphi)\ (1 + \varphi\ /2)$$

κ – Porosity corrected thermal conductivity

κ_m – Uncorrected measured thermal conductivity

φ - Porosity taken from percentage density,

Here $\varphi = 0.1$ (as measured density is 90%)

Table S2 Crystallite size determination using Scherrer analysis

Peak position 2θ (°)	**FWHM β (rad)**	**Crystallite size D (nm)**	**Average D (nm)**
24.40	0.00343	43.21	34.95
29.98	0.00413	36.28	
34.75	0.00433	35.02	
36.92	0.00414	36.89	
49.92	0.00536	29.78	
59.30	0.00584	28.52	
32.44	0.00431	34.95	

Table S3: Thermal conductivity with porosity correction

Temperature (K)	κ_m **(W m^{-1} K^{-1})**	κ_m **(W m^{-1} K^{-1})**	**Porosity corrected** zT	zT
335	0.85	0.89	0.06	0.06
384	0.87	0.92	0.08	0.08
432	0.91	0.96	0.10	0.11
481	0.98	1.03	0.12	0.12
529	0.99	1.04	0.14	0.14
578	0.8	0.84	0.20	0.21
627	0.78	0.82	0.22	0.23
675	0.76	0.80	0.19	0.20
724	0.52	0.55	0.06	0.06

Table S4: *zT* comparison table

Composition	***zT***	**Temperature (K)**	**Reference**
Cu_3SbS_3	0.23	627	This work
Fe doped Cu_3SbS_3	0.70	550-625	6
Tetrahedrite	0.52	600	7
$Mg_{3.2-x}Ce_xSbBi_{0.97}Te_{0.03}$ (x= 0.02)	1.52	723	8
TlCuS	1	573	9
$Bi_{13}S_{18}Br_2$	1	748	10

References

1. J. Rodríguez-Carvajal, J. González-Platas and N. A. Katcho, *Acta Crystallogr., Sect. B*, 2025, **81**, 302–317.
2. A. Sarkar, M. Chakrabarti, S. K. Ray, D. Bhowmick and D. Sanyal, *J. Phys.: Condens. Matter*, 2011, **23**, 155801.
3. H. Luitel, A. Sarkar, M. Chakrabarti, S. Chattopadhyay, K. Asokan and D. Sanyal, *Nucl. Instrum. Methods Phys. Res., Sect. B*, 2016, **379**, 215–218.
4. K. G. Lynn and A. N. Goland, *Solid State Commun.*, 1976, **18**, 1549–1552.
5. D. A. Ferluccio, J. E. Halpin, K. L. MacIntosh, R. J. Quinn, E. Don, R. I. Smith, D. A. MacLaren and J.-W. G. Bos, *J. Mater. Chem. C*, 2019, **7**, 6539–6547.
6. B. Du, R. Zhang, M. Liu, K. Chen, H. Zhang and M. J. Reece, *J. Mater. Chem. C*, 2019, **7**, 394.
7. D. P. Weller and D. T. Morelli, *Front. Electron. Mater.*, 2022, **2**, 913280.
8. L. Zhai, H. Liu, L. Su, Y. Kuang, F. Chen, Y. Zhang, W. Fan and Z. Sun, *Energy Environ. Mater.*, 2025, **8**, e70066
9. A. Bhui, P. V. D. Matukumilli, S. Biswas, A. Ahad, A. Ghata, D. Rawat, M. Dutta, A. Soni, U. V. Waghmare and K. Biswas, *J. Am. Chem. Soc.*, 2025, **147**, 3758–3768.
10. A. Das, K. Debnath, I. Maria, S. Das, P. Dutta, D. Swain, U. V. Waghmare and K. Biswas, *J. Am. Chem. Soc.*, 2024, **146**, 30518–30528.